

Model-independent analysis of new physics effects in $B \rightarrow K_2^*(1430)\mu^+\mu^-$ decay

Ria Sain^{1,*} and Juhi Vardani^{2,†}

¹*Department of Physics, Indian Institute of Technology Guwahati, Assam 781039, India*

²*Indian Institute of Technology Jodhpur, Jodhpur 342037, India*

Recently, the LHCb Collaboration provided updated measurements for the lepton flavour ratios R_K and R_{K^*} . The currently observed values align with the predictions of the standard model. In light of these recent updates, our investigation delves into the repercussions of new physics characterized by universal couplings to electrons and muons. We specifically focus on their impact on various observables within the $B \rightarrow K_2^*(1430)(\rightarrow K\pi)\mu^+\mu^-$ decay. These observables include the differential branching ratio, forward-backward asymmetry (A_{FB}), longitudinal polarization asymmetry (F_L), and a set of optimized observables (P_i). Our findings indicate that the branching ratio of $B \rightarrow K_2^*(\rightarrow K\pi)\mu^+\mu^-$ decay can be suppressed up to 25% for various new physics solutions. Furthermore, all permissible new physics scenarios demonstrate finite enhancement in the muon forward-backward asymmetry (A_{FB}) as well as an increase in the value of the optimized angular observable P_2 . Moreover, in the presence of new physics zero crossing points for A_{FB} and P_2 shift towards higher q^2 . The current data have a mild deviation from SM predictions in P_5' observable in the low- q^2 bin. We also explored massive Z' models, which can generate universal 1D new physics scenarios, characterized by $C_9^{NP} < 0$, $C_{10}^{NP} = -C_9^{NP}$, and $C_9^{NP} = -C_9'$. Using additional constraints coming from $B_s - \bar{B}_s$ mixing and neutrino trident process, we find that the conclusions of the model-independent analysis remain valid.

I. INTRODUCTION

The standard model (SM) of electroweak interactions, by far, provides the meticulous portraiture of fundamental interactions of nature. For all its success, SM can not be considered an impeccable theory. This is because of numerous reasons, for e.g., the particle spectrum of SM is deprived of any dark matter candidates. Further, the CKM mechanism fails to account for the observed matter-anti-matter asymmetry of the universe. Moreover, there is a large number of unpredicted parameters in the SM which are inserted by hand. Therefore, one needs to look for the signatures of possible physics beyond the SM. This can be accomplished in multifarious ways. Flavor physics serves as a fecund tool to hunt for new physics. It capitalizes on the potential of possible heavy new particles to show footprints on decay modes of hadrons and leptons through quantum loops. These decays are accessible at high luminosity low-energy colliders in contrast to the high energy frontier experiments such as ATLAS and CMS. The decays of B mesons are particularly significant because they offer a wealth of observables to probe new physics, including various CP violating observables [1–5]. These are crucial for investigating additional weak phases that could explain the observed matter-antimatter asymmetry. Additionally, these decays have the potential to set limits on physics at much finer length scales [6]. Further, a number of observables in flavour changing neutral current ($b \rightarrow sll$) transition shows deviations with SM predictions, for e.g., branching ratio (BR) of $B_s \rightarrow \phi\mu^+\mu^-$ deviates from the SM prediction at 3.5σ level [7, 8], and the measured value of angular observable

P_5' in $B \rightarrow K^*\mu^+\mu^-$ in $[4.0 - 6.0]GeV^2$ bin, at the level of 3σ [9–12]. These anomalies can be ascribed to new physics (NP) contribution beyond SM in $b \rightarrow s\mu^+\mu^-$ process. Nevertheless, the LHCb collaboration has recently revised the measurements for Lepton flavor universality (LFU) ratio (R_K and R_{K^*}) in $B^0 \rightarrow K_S^0\mu^+\mu^-$ and $B^+ \rightarrow K^{*+}\mu^+\mu^-$ decay modes [13, 14]. The updated results for R_K and R_{K^*} are aligned with SM predictions and provide indications for a universal coupling.

These aberrant measurements can be analyzed in a model-independent way using the language of effective field theory. There are numerous ways in which such analysis can be done. These can be accommodated by NP in the form of vector and axial-vector operators, see for e.g., [3, 15–34]. For e.g., we have several discretions to deal with the hadronic uncertainties and statistical methods. However, it turns out that irrespective of the adopted methodology, the minimal solution requires universal new physics in the form of vector (V) /axial-vector (A) operators. To be more specific, the minimal solution corresponds to a negative value of the Wilson coefficient corresponding to $O_9 \equiv (\bar{s}\gamma^\mu P_L b)(\bar{\mu}\gamma_\mu\mu)$ operator, i.e. all allowed solutions include O_9 operator.

New physics in the form of scalar/pseudoscalar (S/P) or tensor (T) operators are not ruled out. However, they can not accommodate current anomalies by itself. In a specific combination with new physics in the form of V/A operators, S/P or T operators can provide a moderate fit to the data [26, 35]. If at all there is new physics in $b \rightarrow sll$ transition then it should also opine in other decay modes induced by the same quark level transition. There are several such decay modes.

In this work, we consider one such decay $B \rightarrow K_2^*(1430)(\rightarrow K\pi)\ell^+\ell^-$ where K_2^* is a tensor (parity 2^+) meson. Like K^* , the dominant decay mode of K_2^* is a two-body $K\pi$ mode which is easily accessible at the

* ria.sain.2013@gmail.com

† vardani.1@iitj.ac.in

LHCb. Given the similarity between $B \rightarrow K^* \ell^+ \ell^-$ and $B \rightarrow K_2^*(1430) \ell^+ \ell^-$ decay modes and the fact that $B \rightarrow K_2^*(1430) \gamma$ decay has already been observed by the Belle and BABAR collaborations [36, 37], one can expect measurement of $B \rightarrow K_2^*(1430) \ell^+ \ell^-$ decay mode at the LHCb or Belle-II. The form factor for $B \rightarrow K_2^*$ transition, which is non-perturbative, has been computed using various approaches. These includes: ISGW [38], ISGW2 model [39, 40], Perturbative QCD [41], Light Cone Sum Rule [42], and large energy effective theory (LEET) approach [43]. Using different form factors $B \rightarrow K_2^*(1430) \ell^+ \ell^-$ decay has been extensively analyzed within SM as well as in various beyond SM scenarios. The scrutiny span across several references including but not limited to [44–54]. For instance in ref. [50] $B \rightarrow K_2^* \mu \mu$ decay has been examined in SM along with vector-like quark model and family non-universal Z' model. Additionally, ref. [49] delves into light Z' model considering coupling emerges from C_9^{NP} *i.e.* vectorial contribution to muon and get remarkable contribution to optimized observable (P'_5) and flavor difference observable (Q_i) defined in ref. [49] for NP. Furthermore, the decay $B \rightarrow K_2^* \ell \ell$ has also been investigated with flipped sign of C_7^{eff} and universal extra-dimensional model as in ref.[44]. Ref. [46] investigates the impact of new V/A, S/P, and T type interaction on $B \rightarrow K_2^* \mu \mu$ decay. Recently, LHCb collaboration has provided updated measurements for R_K and R_K^* [13, 14], which are consistent with SM predictions. In this work, we exploit the LCSR and LEET to ascertain the transition form factor for $B \rightarrow K_2^*$ transition, and we conduct a comprehensive analysis of $B \rightarrow K_2^*(1430)(\rightarrow K\pi) \ell^+ \ell^-$ decay, taking into account new physics in the form of V/A and S/P operators, considering scenarios with non-vanishing lepton masses. In most of works, the $B \rightarrow K_2^*(1430)(\rightarrow K\pi) \ell^+ \ell^-$ decay has been scrutinized with non universal coupling. However, in the presence of universal Wilson coefficients(WCs), universal coupling will induce new physics effects in $b \rightarrow s \mu^+ \mu^-$ decay. For various universal NP solutions, we study basic observables

in $B \rightarrow K_2^*(1430)(\rightarrow K\pi) \mu^+ \mu^-$ decay modes such as the branching ratio BR , muon forward-backward asymmetry A_{FB} , K_2^* longitudinal polarization fraction F_L and optimized observables (P_i). It would be interesting to see whether the current data allows for a sizeable new physics effects in some of $B \rightarrow K_2^*(1430)(\rightarrow K\pi) \ell^+ \ell^-$ observables. We investigate whether these observables can discriminate between some of the allowed new physics solutions.

In addition, we study this decay in the Z' model, it has potential to employ these model-independent solutions at tree level. In model-independent analysis, $b \rightarrow s ll$ transition gives constraints. However, in Z' $B_s - \bar{B}_s$ mixing and neutrino trident also give additional constraints. We investigate Wilson coefficients in Z' for different scenarios and predict angular observables for $B \rightarrow K_2^*(1430) \mu^+ \mu^-$ in Z' model.

The paper is organized as follows. In section II, we start with effective Hamiltonian for $b \rightarrow s l^+ l^-$ transition for SM and NP. Furthermore, we also present the hadronic matrix element for $B \rightarrow K_2^*$ transition. In section III we discussed $B \rightarrow K_2^*$ transition form factor using different techniques. In section IV we calculate fourfold distribution for $B \rightarrow K_2^*(K_2^* \rightarrow K\pi) ll$ for vector, axial-vector and scalar interaction. In section V we study the SM and NP predictions for angular observables $B \rightarrow K_2^*(\rightarrow K\pi) ll$ decay and the effect of different form factors on these. Further, we investigate the sensitivity of these observables to discriminate various NP solutions. In section VIII we provide Z' model-dependent analysis for $B \rightarrow K_2^* \mu^+ \mu^-$ decay. In section VIII we provide a summary of our results.

II. THEORETICAL FRAMEWORK

The decay $B \rightarrow K_2^*(1430) \mu^+ \mu^-$ is mediated by the $b \rightarrow s \mu^+ \mu^-$ quark level transition. In the SM, the effective Hamiltonian for $b \rightarrow s \mu^+ \mu^-$ transition is given by

$$\mathcal{H}^{\text{SM}} = -\frac{4G_F}{\sqrt{2}\pi} V_{ts}^* V_{tb} \left[\sum_{i=1}^6 C_i(\mu) \mathcal{O}_i(\mu) + C_7^{\text{eff}} \frac{e}{16\pi^2} [\bar{s} \sigma_{\mu\nu} (m_s P_L + m_b P_R) b] F^{\mu\nu} + C_9^{\text{eff}} \frac{\alpha_{em}}{4\pi} (\bar{s} \gamma^\mu P_L b) (\bar{\mu} \gamma_\mu \mu) \right] + C_{10} \frac{\alpha_{em}}{4\pi} (\bar{s} \gamma^\mu P_L b) (\bar{\mu} \gamma_\mu \gamma_5 \mu), \quad (1)$$

where G_F is Fermi constant, V_{tb} , V_{ts} are the CKM matrix elements, C_i are Wilson coefficients, $P_{L,R} = (1 \mp \gamma^5)/2$ are the projection operators and $\mathcal{O}_i(\mu)$ are four fermion operators. The effect of the operators \mathcal{O}_i , $i = 1 - 6, 8$ embedded in the redefined effective Wilson coefficients $C_7(\mu) \rightarrow C_7^{\text{eff}}(\mu, q^2)$ and $C_9(\mu) \rightarrow C_9^{\text{eff}}(\mu, q^2)$. These redefined effective Wilson coefficients are described in Appendix I [56]. The SM values of the Wilson coefficients

can be found in Ref. [57]. In a model-independent approach, we can add possible vector(V), axial-vector(A), scalar(S), and pseudo-scalar(P) new physics contributions to the SM effective Hamiltonian. The NP Hamiltonian

nian can be expressed as

$$\begin{aligned} \mathcal{H}_{\text{VA}}^{\text{NP}} = & -\frac{\alpha_{\text{em}} G_F}{\sqrt{2}\pi} V_{ts}^* V_{tb} [C_9^{\text{NP}} (\bar{s}\gamma^\mu P_L b) (\bar{\mu}\gamma_\mu \mu) \\ & + C_{10}^{\text{NP}} (\bar{s}\gamma^\mu P_L b) (\bar{\mu}\gamma_\mu \gamma_5 \mu) + C_9' (\bar{s}\gamma^\mu P_R b) (\bar{\mu}\gamma_\mu \mu) \\ & + C_{10}' (\bar{s}\gamma^\mu P_R b) (\bar{\mu}\gamma_\mu \gamma_5 \mu)], \end{aligned} \quad (2)$$

$$\begin{aligned} \mathcal{H}_{\text{SP}}^{\text{NP}} = & -\frac{\alpha_{\text{em}} G_F}{\sqrt{2}\pi} V_{ts}^* V_{tb} [C_S (\bar{s} P_R b) (\bar{\mu}\mu) + C_P (\bar{s} P_R b) (\bar{\mu}\gamma_5 \mu) \\ & + C_S' (\bar{s} P_L b) (\bar{\mu}\mu) + C_P' (\bar{s} P_L b) (\bar{\mu}\gamma_5 \mu)], \end{aligned}$$

where $C_{9,10}^{\text{NP}}$, $C_{9,10}'$, and $C_{S,P}'$ are the NP Wilson coefficients.

A. Hadronic matrix elements

The $B \rightarrow K_2^*(1430)\ell^+\ell^-$ decay consists of both short-distance and long-distance physics. The short distance physics is embedded in the Wilson coefficients whereas the long distance contribution can be expressed in terms of hadronic matrix elements. For $B \rightarrow K_2^*$ transition, the hadronic matrix elements for V and A currents can be parameterized in terms of four form factors $V(q^2)$ and $A_{0,1,2}(q^2)$. These can be written as [41, 42]

$$\langle K_2^*(k, \epsilon^*) | \bar{s}\gamma^\mu b | \bar{B}(p) \rangle = -\frac{2V(q^2)}{m_B + m_{K_2^*}} \epsilon^{\mu\nu\rho\sigma} \epsilon_{T\nu}^* p_\rho k_\sigma,$$

$$\begin{aligned} \langle K_2^*(k, \epsilon^*) | \bar{s}\gamma^\mu \gamma_5 b | \bar{B}(p) \rangle = & 2im_{K_2^*} A_0(q^2) \frac{\epsilon_T^* \cdot q}{q^2} q^\mu \\ & + i(m_B + m_{K_2^*}) A_1(q^2) \\ & [\epsilon_T^{*\mu} - \frac{\epsilon_T^* \cdot q}{q^2} q^\mu] - iA_2(q^2) \\ & \frac{\epsilon_T^* \cdot q}{m_B + m_{K_2^*}} [(p+k)^\mu \\ & - \frac{m_B^2 - m_{K_2^*}^2}{q^2} q^\mu], \end{aligned}$$

$$\langle K_2^*(k, \epsilon^*) | \bar{s}q_\nu \sigma^{\mu\nu} b | \bar{B}(p) \rangle = -2iT_1 \epsilon^{\mu\nu\rho\sigma} \epsilon_{T\nu}^* p_\rho k_\sigma,$$

$$\begin{aligned} \langle K_2^*(k, \epsilon^*) | \bar{s}q_\nu \sigma^{\mu\nu} \gamma_5 b | \bar{B}(p) \rangle = & T_2 [(m_B^2 - m_{K_2^*}^2) \epsilon_{T\mu}^* \\ & - (\epsilon^* \cdot q) P^\mu] \\ & + T_3 (\epsilon^* \cdot q) [q^\mu - \frac{q^2 (p+k)^\mu}{m_B^2 - m_{K_2^*}^2}]. \end{aligned} \quad (3)$$

However, it can be shown that the matrix element of $B \rightarrow K_2^*$ transition mediated by scalar current ($\bar{s}b$) vanishes and the pseudo-scalar interaction leads to

$$\langle K_2^*(k, \epsilon^*) | \bar{s}\gamma_5 b | \bar{B}(p) \rangle = -\frac{2im_{K_2^*} A_0(q^2)}{m_b + m_s} (\epsilon_T^* \cdot q), \quad (4)$$

where p and k are the momentum of B and K_2^* meson, respectively. The polarization $\epsilon^{\mu\nu}(n)$ of tensor meson K_2^* , which has four momentum $(k_0, 0, 0, \vec{k})$, can be written in terms of the spin-1 polarization vectors [41, 50, 55]

$$\begin{aligned} \epsilon_{\mu\nu}(\pm 2) &= \epsilon_\mu(\pm 1)\epsilon_\nu(\pm 1), \\ \epsilon_{\mu\nu}(\pm 1) &= \frac{1}{\sqrt{2}} [\epsilon_\nu(\pm)\epsilon_\mu(0) + \epsilon_\nu(\pm)\epsilon_\mu(0)], \\ \epsilon_{\mu\nu}(0) &= \frac{1}{\sqrt{6}} [\epsilon_\mu(+)\epsilon_\nu(-) + \epsilon_\nu(+)\epsilon_\mu(-)] \\ &+ \sqrt{\frac{2}{3}} \epsilon_\mu(0)\epsilon_\nu(0), \end{aligned} \quad (5)$$

where the spin-1 polarization vectors are defined as [58, 59]:

$$\epsilon_\mu(0) = \frac{1}{m_{K_2^*}} (\vec{k}_z, 0, 0, k_0), \quad \epsilon_\mu(\pm) = \frac{1}{\sqrt{2}} (0, 1, \pm i, 0). \quad (6)$$

We are studying the decay mode where we have two leptons in the final state makes the virtual particle to have $n = 0, \pm 1$ helicity states, so in this case, the $n = \pm 2$ helicity states of the K_2^* is not realized. Therefore, a new polarization vector is introduced which behave very similar to spin 1 polarisation vector.[60]:

$$\epsilon_{T\mu}(h) = \frac{\epsilon_{\mu\nu} p^\nu}{m_B}. \quad (7)$$

The explicit expressions of polarization vectors are

$$\begin{aligned} \epsilon_{T\mu}(\pm 1) &= \frac{1}{m_B} \frac{1}{\sqrt{2}} \epsilon(0) \cdot p \epsilon_\mu(\pm) \\ &= \frac{\sqrt{\lambda}}{\sqrt{8}m_B m_{K_2^*}} \epsilon_\mu(\pm), \\ \epsilon_{T\mu}(0) &= \frac{1}{m_B} \sqrt{\frac{2}{3}} \epsilon(0) \cdot p \epsilon_\mu(0) \\ &= \frac{\sqrt{\lambda}}{\sqrt{6}m_B m_{K_2^*}} \epsilon_\mu(0). \end{aligned} \quad (8)$$

The virtual gauge boson can have, longitudinal, transverse and time-like, polarization states as

$$\begin{aligned} \epsilon_V^\mu(0) &= \frac{1}{\sqrt{q^2}} (-|\vec{q}_z|, 0, 0, -q_0), \quad \epsilon_V^\mu(\pm) = \frac{1}{\sqrt{2}} (0, 1, \pm i, 0) \\ \epsilon_V^\mu(t) &= \frac{1}{\sqrt{q^2}} (q_0, 0, 0, q_z) \end{aligned} \quad (9)$$

where $q^\mu = (q_0, 0, 0, q_z)$ is four momentum of gauge boson.

III. $B \rightarrow K_2^*$ TRANSITION FORM FACTOR

The hadronic matrix element which is involved in the exclusive B mesons decay comprises several form factors, which are non-perturbative entities. These are the most significant contributors to the uncertainty in theoretical predictions. The hadronic matrix elements for V and A currents, for $B \rightarrow K_2^*$ transition, can be parameterized in terms of four form factors, $V(q^2)$ and $A_{0,1,2}(q^2)$. They can be calculated using a variety of techniques, some of which include perturbative lattice QCD [41], QCD Sum Rules, and the Light Cone Sum Rule(LCSR) [42, 60–62]. The large energy effective theory (LEET) and LCSR have been considered for the form factor determination. Under LCSR three distinct parameters can be used to describe the q^2 distribution for the B to T transition [42]:

$$F^{B_q T}(q^2) = \frac{F^{B_q T}(0)}{1 - a(q^2/m_B^2) + b(q^2/m_B^2)^2}. \quad (10)$$

where $F^{B_q T}$ can be $V^{BK_2^*}$, $A_{0,1,2}^{BK_2^*}$ or $T_{1,2,3}^{BK_2^*}$. The form factor at zero recoil is denoted here by $F^{B_q T}(0)$, a and b are considered to be input parameters, and their respective numeric values are given in TableVII. The decay constant of the concerned meson, the mass of the b quark, the Borel mass, and the mass of the strange quark are the sources of error in the form factor. Within bounds of bulky quark mass $m_b \rightarrow \infty$ and enormous energy of final hadron ($E \rightarrow \infty$), $B \rightarrow K_2^*$ interaction can be expanded in small ratio $\frac{\lambda_{QCD}}{E}$ and $\frac{\lambda_{QCD}}{m_b}$. In this limit, energy symmetry is achieved at leading power in $\frac{1}{m_b}$, this symmetry significantly simplifies the heavy to light transition [43, 63] and reduces the uncertainty in angular observables. In the large recoil energy domain, the $B \rightarrow K_2^*$ transition form factor can be formulated in two independent universal soft form factors, $\zeta_{\perp}(q^2)$ and $\zeta_{\parallel}(q^2)$. All the form factors associated with $B \rightarrow K_2^*$ transition can be explored in terms of $\zeta_{\perp}(q^2)$ and $\zeta_{\parallel}(q^2)$ as well [52, 53]

$$A_0(q^2) = \frac{m_{K_2^*}}{|p_{K_2^*}|} \left[\left(1 - \frac{m_{K_2^*}^2}{m_B} \right) \zeta_{\parallel}(q^2) + \frac{m_{K_2^*}}{m_B} \zeta_{\perp}(q^2) \right],$$

$$A_1(q^2) = \frac{m_{K_2^*}}{|p_{K_2^*}|} \frac{2E_{K_2^*}}{m_B + m_{K_2^*}} \zeta_{\perp}(q^2),$$

$$A_2(q^2) = \frac{m_{K_2^*}}{|p_{K_2^*}|} \left(1 - \frac{m_{K_2^*}}{m_B} \right) \left[\zeta_{\perp}(q^2) - \frac{m_{K_2^*}}{E} \zeta_{\parallel}(q^2) \right],$$

$$V(q^2) = \frac{m_{K_2^*}}{|p_{K_2^*}|} \left(1 - \frac{m_{K_2^*}}{m_B} \right) \zeta_{\perp}(q^2),$$

$$T_1(q^2) = \frac{m_{K_2^*}}{|p_{K_2^*}|} \zeta_{\perp}(q^2),$$

$$T_2(q^2) = \frac{m_{K_2^*}}{|p_{K_2^*}|} \zeta_{\perp}(q^2) \left(1 - \frac{q^2}{m_B^2 - m_{K_2^*}^2} \right),$$

$$T_3(q^2) = \frac{m_{K_2^*}}{|p_{K_2^*}|} \left[\zeta_{\perp} - \left(1 - \frac{m_{K_2^*}^2}{m_B^2} \right) \frac{m_{K_2^*}}{E} \zeta_{\parallel}(q^2) \right].$$

The q^2 reliance of the soft form factors $\zeta_{\perp}(q^2)$ and $\zeta_{\parallel}(q^2)$ is given by [43, 52],

$$\zeta_{\parallel,\perp}(q^2) = \frac{\zeta_{\parallel,\perp}(0)}{(1 - q^2/m_B^2)^2}. \quad (11)$$

Here $\zeta_{\parallel,\perp}(0)$ are form factors at zero momentum transfer. There are several tools to calculate form factors at zero recoil, The Bauer-Stech-Wirbel (BSW) model is one of the tools that might be employed to calculate form factors at zero recoil [52, 64]. Here, we applied it to determine the form factor at zero recoil. The values derived with the perturbative QCD technique [41] using the non-trivial relations observed at the large energy limit have been used for our numerical analysis. These values are $\zeta_{\parallel}(0) = 0.26 \pm 0.10$ and $\zeta_{\perp}(0) = 0.29 \pm 0.09$.

IV. FOURFOLD ANGULAR DISTRIBUTION

The differential distribution of four-body decay $B \rightarrow K_2^*(\rightarrow K\pi)\ell^+\ell^-$ can be parametrized as the function of one kinematic and three angular variables. The kinematic variable is $q^2 = (p - k)^2$, where p and k are four-momenta of B and K_2^* mesons respectively. The K_2^* is moving in the Z direction in the B rest frame. The angular variables are defined in the lepton rest frame. They are (a) θ_K the angle between K_2^* and K mesons where K meson comes from K_2^* decay, (b) θ_{ℓ} the angle between momenta of ℓ^- and K_2^* meson and (c) ϕ the angle between K_2^* decay plane and the plane defined by the dilepton momenta. Summing over the spins of final state particles, one can obtain the full decay distribution as [50, 65, 66].

$$\begin{aligned}
\frac{d^4\Gamma}{dq^2 d \cos \theta_\ell d \cos \theta_K d\phi} &= \frac{15}{128\pi} [I_1^c (3 \cos^2 \theta_K - 1)^2 + I_1^s 3 \sin^2 2\theta_K + I_2^c (3 \cos^2 \theta_K - 1)^2 \cos 2\theta_\ell + I_2^s 3 \sin^2 2\theta_K \cos 2\theta_\ell \\
&+ I_3 3 \sin^2 2\theta_K \sin^2 \theta_\ell \cos 2\phi + I_4 2\sqrt{3} (3 \cos^2 \theta_K - 1) \sin 2\theta_K \sin 2\theta_\ell \cos \phi \\
&+ I_5 2\sqrt{3} (3 \cos^2 \theta_K - 1) \sin 2\theta_K \sin \theta_\ell \cos \phi + I_6^s 3 \sin^2 2\theta_K \cos \theta_\ell + I_6^c (3 \cos^2 \theta_K - 1)^2 \cos \theta_\ell \\
&+ I_7 2\sqrt{3} (3 \cos^2 \theta_K - 1) \sin 2\theta_K \sin \theta_\ell \sin \phi + I_8 2\sqrt{3} (3 \cos^2 \theta_K - 1) \sin 2\theta_K \sin 2\theta_\ell \sin \phi \\
&+ I_9 3 \sin^2 2\theta_K \sin^2 \theta_\ell \sin 2\phi].
\end{aligned} \tag{12}$$

The angular coefficients I_i 's in the equation 12 are function of q^2 , which can be written in terms of various transversity amplitudes as:

$$\begin{aligned}
I_1^c &= (|A_{0L}|^2 + |A_{0R}|^2) + \frac{8m_\ell^2}{q^2} \text{Re} [A_{0L}A_{0R}^*] + 4\frac{m_\ell^2}{q^2} |A_t|^2 \\
&+ (\beta_\ell^2 |A_S|^2), \\
I_1^s &= \frac{3}{4} \left(1 - \frac{4m_\ell^2}{3q^2}\right) [|A_{\perp L}|^2 + |A_{\parallel L}|^2 + L \Leftrightarrow R] \\
&+ \frac{4m_\ell^2}{q^2} \text{Re} [A_{\perp L}A_{\perp R}^* + A_{\parallel L}A_{\parallel R}^*], \\
I_2^c &= -\beta_\ell^2 [|A_{0L}|^2 + |A_{0R}|^2], \\
I_2^s &= \frac{\beta_\ell^2}{4} [|A_{\perp L}|^2 + |A_{\parallel L}|^2 + L \Leftrightarrow R], \\
I_3 &= \frac{\beta_\ell^2}{2} [(|A_{\perp L}|^2 - |A_{\parallel L}|^2 + L \Leftrightarrow R)], \\
I_4 &= \frac{\beta_\ell^2}{\sqrt{2}} \text{Re} [A_{0L}A_{\parallel L}^* + A_{0R}A_{\parallel R}^*], \\
I_5 &= \sqrt{2}\beta_\ell \text{Re} [A_{0L}A_{\perp L}^* - A_{0R}A_{\perp R}^*], \\
I_6^s &= -2\beta_\ell \text{Re} [A_{\parallel L}A_{\perp L}^* - A_{\parallel R}A_{\perp R}^*], \\
I_6^c &= 4\beta_\ell \text{Re} \left[\frac{m_\ell}{\sqrt{q^2}} (A_{0L} + A_{0R}) A_S^* \right], \\
I_7 &= -\sqrt{2}\beta_\ell \text{Im} \left[A_{0L}A_{\parallel L}^* - A_{0R}A_{\parallel R}^* \right. \\
&\left. + \frac{m_\ell}{\sqrt{q^2}} (A_{\perp L}^* + A_{\perp R}^*) A_S \right], \\
I_8 &= \frac{\beta_\ell^2}{\sqrt{2}} \text{Im} [(A_{0L}A_{\perp L}^* + A_{0R}A_{\perp R}^*)], \\
I_9 &= \beta_\ell^2 \text{Im} \left[(A_{\parallel L}^*A_{\perp L} + A_{\parallel R}^*A_{\perp R}) \right],
\end{aligned} \tag{13}$$

where $\beta_i = \sqrt{1 - 4m_i^2/q^2}$.

From the angular distribution, one can derive observables such as the forward-backward asymmetry A_{FB} and the differential decay width $d\Gamma/dq^2$ as a function of the dilepton invariant mass q^2 as defined in [49, 50, 65].

- The differential decay width $d\Gamma/dq^2$ can be determined by integrating over the angles θ_l, θ_k , and, ϕ as [50, 65]:

$$\frac{d\Gamma}{dq^2} = \frac{1}{4} (3I_1^c + 6I_1^s - I_2^c - 2I_2^s). \tag{14}$$

- The forward-backward asymmetry of lepton pair A_{FB} (normalized by differential decay width) is given by [50, 65],

$$A_{\text{FB}}(q^2) = \left[\int_0^1 - \int_{-1}^0 \right] d \cos \theta \frac{d^2\Gamma}{dq^2 d \cos \theta_l}, \tag{15}$$

$$\frac{d\bar{A}_{\text{FB}}}{dq^2} = \frac{3I_6}{3I_1^c + 6I_1^s - I_2^c - 2I_2^s}. \tag{16}$$

- Similarly fourfold distribution for CP conjugate process $\bar{B} \rightarrow \bar{K}_2^*(\bar{K}_2^* \rightarrow K\pi)l^+l^-$ is given as:

$$\frac{d^4\Gamma}{dq^2 d \cos \theta_\ell d \cos \theta_K d\phi} = \frac{15}{128\pi} \sum_{i=1}^9 \bar{I}_i(q^2, \theta_l, \theta_k, \phi)$$

Since CP transformation interchange lepton and antilepton, leads to a transformation $\theta_l \rightarrow \theta_l - \pi$, and $\phi \rightarrow -\phi$. This leads to $I_{1,2,3,4,7}^{(a)} \rightarrow \bar{I}_{1,2,3,4,7}^{(a)}$, $I_{5,6,8,9}^{(a)} \rightarrow -\bar{I}_{5,6,8,9}^{(a)}$. One can construct optimized observables with reduced uncertainty as defined in Refs. [67, 68]:

$$\begin{aligned}
\langle P_1 \rangle &= \frac{1}{2} \frac{\int dq^2 I_3}{\int dq^2 I_2^s}, & \langle P_2 \rangle &= \frac{1}{8} \frac{\int dq^2 I_6^s}{\int dq^2 I_2^s}, \\
\langle P_4' \rangle &= \frac{\int dq^2 I_4}{\sqrt{-\int dq^2 I_2^s \int dq^2 I_2^c}}, \\
\langle P_5' \rangle &= \frac{\int dq^2 I_5}{2\sqrt{-\int dq^2 I_2^s \int dq^2 I_2^c}}
\end{aligned} \tag{17}$$

V. ANALYSIS OF $B \rightarrow K_2^*(1430)(\rightarrow K\pi)l^+l^-$: A MODEL INDEPENDENT APPROACH

In this segment, prediction for a number of angular observables is done for $B \rightarrow K_2^*(1430)(\rightarrow K\pi)l^+l^-$ decay

for low q^2 within SM and different NP scenarios. In the expression of decay rate and other angular observables, the scalar and pseudoscalar amplitudes are suppressed by lepton mass as in angular coefficients I_i . These operators are heavily constrained from $B_s \rightarrow \mu^\pm \mu^\mp$ decay [69, 70]. In our analysis, we are considering $B \rightarrow K_2^*(1430)(\rightarrow K\pi)\mu^+\mu^-$ for the smallness of the mass of $m_l = m_\mu$, the contribution of the scalar operators are negligible. So, we analyzed $B \rightarrow K_2^*(1430)(\rightarrow K\pi)\mu^+\mu^-$ decay without taking them. We focus on NP scenarios which comprises of either one or two non-zero Wilson Coefficients. Choosing low q^2 region as $1 \leq q^2 \leq 6$ GeV², we provide angular observable predictions for the $B \rightarrow K_2^*(1430)(\rightarrow K\pi)\mu^+\mu^-$ decay by employing two distinct sets of form factors for $B \rightarrow K_2^*$ transition. The relevant numeric expressions of form factors are given in eqn. [10, 11], Table VII provides the estimated value of fit parameters for these form factors. Our goal is to scrutinize observables for $B \rightarrow K_2^*(1430)(\rightarrow K\pi)\mu^+\mu^-$ within various New Physics scenarios and look for deviation from SM predictions.

Considering recent flavour anomalies like $B_s \rightarrow \mu^+\mu^-$ [34, 71–75], $B_s \rightarrow \phi\mu^+\mu^-$ [7, 8], the global fit was performed by several groups to all $b \rightarrow s\mu^+\mu^-$ data for determining the pattern of Wilson coefficients which provides a good fit to data. These fit suggest that several scenarios can mitigate tension between experimental data and theory. We consider three scenarios, considering one operator or two related operators at a time. These correspond to vectorial C_9^{NP} , $C_9'^{NP}$, and axial vectorial C_{10}^{NP} contribution to muon. Before December 2022 updates, real fit for $b \rightarrow s\mu^+\mu^-$ shows that C_9^{NP} , and $C_9^{NP} = -C_{10}^{NP}$ provide a good fit to data. Whereas $C_9^{NP} = -C_9'^{NP}$ provides a moderate fit [28]. In ref [34], it was shown that along with these, a moderate solution C_{10}^{NP} can also explain B anomalies.

Solutions	Wilson coefficients	1σ range
S1	C_9^{NP}	-1.08 ± 0.18
S2	$C_9^{NP} = -C_{10}^{NP}$	-0.50 ± 0.12
S3	$C_9^{NP} = -C_9'^{NP}$	-0.88 ± 0.16

TABLE I: Universal NP scenarios suggested as an explanation for all $b \rightarrow sl^+l^-$ anomalies. The numeric value of the Wilson coefficients is taken from [31].

However, updated fit after considering updated measurement for R_K , R_K^* by LHCb December 2022 [13] [14] alongside the latest measurement of branching ratio $B_s \rightarrow \mu^+\mu^-$ [77] and several observables for $B_s \rightarrow \phi\mu^+\mu^-$ by CMS[8] suggest that non universal coupling $C_{9/10}^V$ i.e. $b \rightarrow s\mu^+\mu^-$ is disfavored [31]. The alignment of the updated LHCb measurements R_K , R_K^* (LHCb) with Standard Model predictions indicates a potential preference for universal coupling in $b \rightarrow sl\ell$ transitions. Results after considering universal Wilson Coefficients still supports C_9^{NP} is the best scenario, and $C_9^{NP} = -C_9'^{NP}$, $C_9^{NP} = -C_{10}^{NP}$ to be a good solution as shown in Table I.

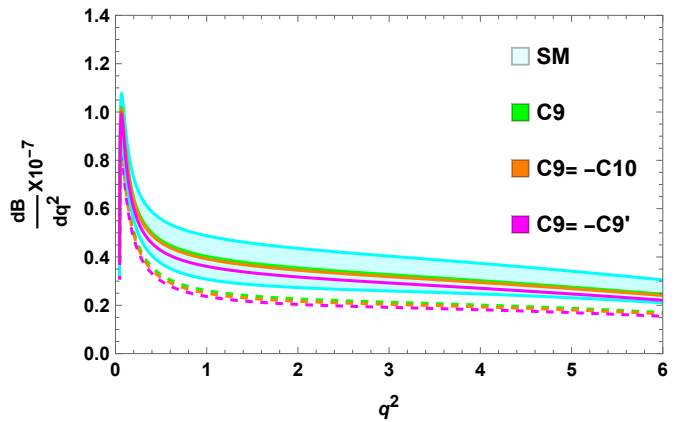


FIG. 1: Plot for q^2 distribution in SM as well as for several new physics scenarios for branching ratio of $B \rightarrow K_2^*(\rightarrow K\pi)\mu^+\mu^-$ decay. The standard model is denoted with the cyan band. The solid and dotted lines represent the maximum and minimum boundaries for each new physics scenario.

Further, we anticipate q^2 dependency of the angular observables using all input parameters, including V_{CKM} matrix element and Wilson coefficients that are listed in Table VI and Ref. [57] respectively. Table II shows the observable central value and corresponding 1σ uncertainties for all observables like differential branching ratio, the normalized forward-backward asymmetry A_{FB} , Longitudinal polarization fraction F_L , and for optimized observables such as $P'_{4,5}$ and $P_{1,2}$ for $1 \leq q^2 \leq 6$ GeV². The third column comprised of the integrated observables using LCSR form factor and $B \rightarrow K_2^*$ transition at large recoil within SM. The result of different choices of form factors have a considerable impact on the angular observables, this can be seen from Table II, where the angular observables have been predicted for SM and different NP scenarios at $\mu = 4.2$ GeV. In appendix Fig.7 suggests that within standard model branching ratio (BR) for $B \rightarrow K_2^*(\rightarrow K\pi)\ell^+\ell^-$ ($\ell = \mu$) decay with LCSR form factor have a significant q^2 deviation from BR using LEET form factor formulation. In Fig2, we present q^2 dependency for these observables in low dilepton mass region, $[0.045, 6.0]$ GeV² for SM and different NP scenarios following LCSR form factor.

The branching ratio BR, angular observables F_L , A_{FB} and optimized angular observables $P_{1,2}$, $P'_{4,5}$ computed for the three updated NP scenarios in low $q^2 \in [1, 6]$ GeV² as listed in Table II and compared with SM for LCSR formulation in low q^2 . In Fig1, we show the behavior of branching ratio with q^2 for SM and NP scenarios with LCSR form factor. This is also evident from Fig.1 that after updated measurements of R_K , R_K^* there is suppression in branching ratio for universal Wilson Coefficients in $b \rightarrow sl^+\ell^-$ ($\ell = e, \mu$). It is apparent from Table II that the branching ratio for $B \rightarrow K_2^*(1430)\mu^+\mu^-$ is the order of $O(10^{-7})$ in SM as well as for all the NP scenarios. For the S1 scenario, there is a suppression in the

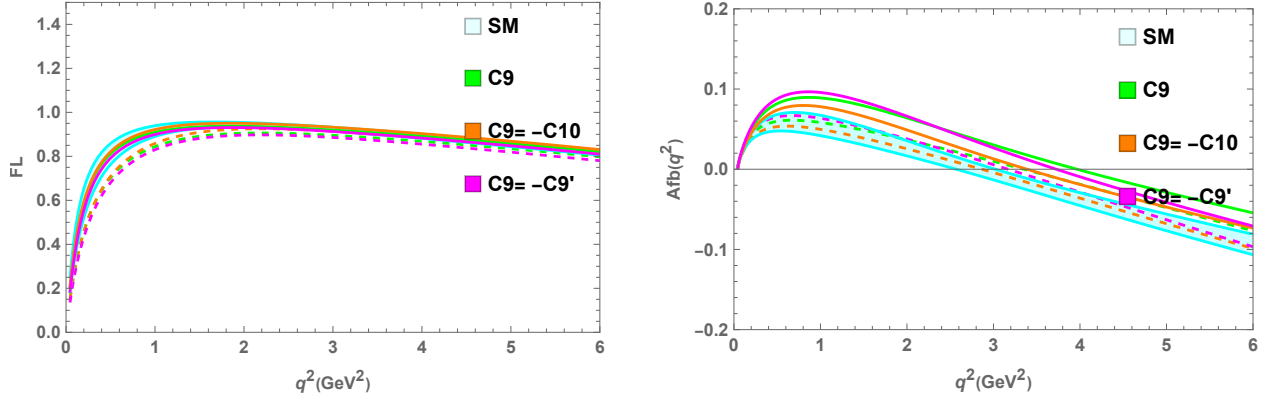


FIG. 2: The figure delineate q^2 dependency for Longitudinal Polarization F_L and forward-backward asymmetry (A_{FB}) for $B \rightarrow K_2^*(\rightarrow K\pi)\mu^+\mu^-$ decay Within the confines of the Standard Model and across various new physics scenarios. The solid and dotted lines represent the maximum and minimum boundaries for each new physics scenario.

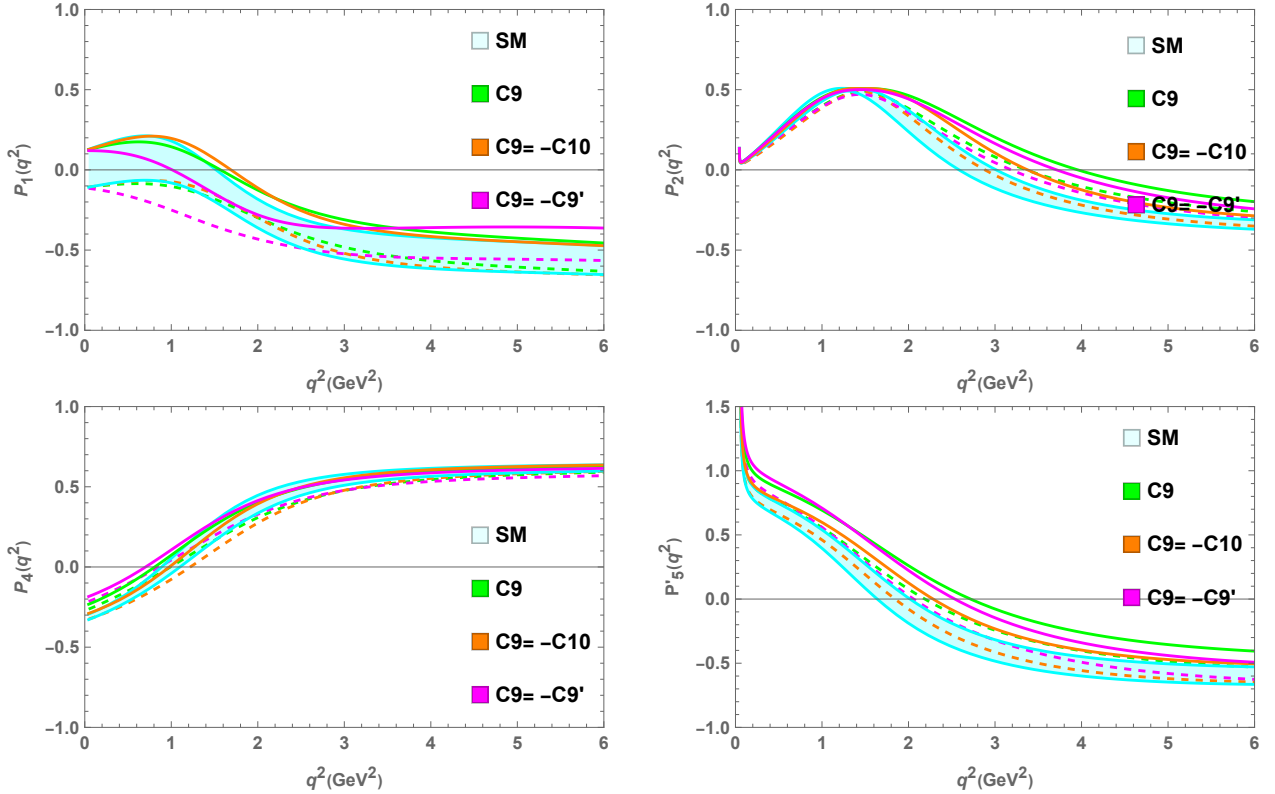


FIG. 3: Plots for q^2 distribution in SM as well as for several new physics scenarios for optimized angular observables P_1, P_4 left pannel and P_2, P_5 right pannel for $B \rightarrow K_2^*\mu^+\mu^-$ decay. The standard model is filled with the cyan band. The solid and dotted lines represent the maximum and minimum boundaries for each new physics scenario.

value of branching ratio of nearly about $\sim 15\%$. Furthermore, scenarios S2 and S3 lead to a larger suppression up to 25% from the SM value as compared to scenario S1.

Forward-backward asymmetry (A_{FB}) has a zero crossing for SM as well as for NP. Furthermore, in the presence of NP it shifted towards high q^2 . A_{FB} is positive for $q^2 < q_0^2$ and negative for $q^2 > q_0^2$ as shown in Fig.2,

where q_0 is corresponding value of q^2 at zero crossing point. We also give A_{FB} predictions for $q^2 < q_0^2$ as well as for $q^2 > q_0^2$ as shown in TableIII. From the right of Fig2, it is clear that new physics can enhance forward-backward asymmetry A_{FB} of muon from SM predictions. For all NP scenarios, the K_2^* longitudinal polarization (F_L) for the low di-lepton mass square, renders the val-

Angular Observable	Form factor	SM	S1	S2	S3
$BR \times 10^7$	LCSR	1.554 ± 0.558	1.2696 ± 0.446	1.2204 ± 0.446	1.136 ± 0.392
	LEET	1.212 ± 0.605	1.041 ± 0.515	0.967 ± 0.484	0.959 ± 0.471
F_L	LCSR	0.835 ± 0.016	0.821 ± 0.021	0.8234 ± 0.0193	0.811 ± 0.023
	LEET	0.721 ± 0.105	0.689 ± 0.116	0.715 ± 0.108	0.667 ± 0.123
A_{FB}	LCSR	-0.015 ± 0.011	0.0087 ± 0.015	-0.0053 ± 0.013	0.00419 ± 0.015
	LEET	-0.050 ± 0.026	0.0 ± 0.012	-0.028 ± 0.015	-0.007 ± 0.012
P_1	LCSR	-0.446 ± 0.149	-0.389 ± 0.142	-0.414 ± 0.146	-0.406 ± 0.135
	LEET	0.374 ± 0.001	-0.008 ± 0.065	0.219 ± 0.047	-0.003 ± 0.060
P_2	LCSR	-0.112 ± 0.086	0.056 ± 0.089	-0.039 ± 0.096	0.0247 ± 0.092
	LEET	-0.171 ± 0.001	0.018 ± 0.032	-0.093 ± 0.023	-0.018 ± 0.028
P'_4	LCSR	0.975 ± 0.111	0.934 ± 0.114	0.921 ± 0.125	0.932 ± 0.104
	LEET	0.879 ± 0.010	0.840 ± 0.011	0.823 ± 0.0161	0.832 ± 0.012
P'_5	LCSR	-0.349 ± 0.137	-0.138 ± 0.139	-0.274 ± 0.146	-0.201 ± 0.151
	LEET	-0.548 ± 0.0032	-0.302 ± 0.049	-0.470 ± 0.027	-0.383 ± 0.045

TABLE II: Angular Observables SM and NP predictions with 1σ for q^2 [1-6] GeV^2 bin following LCSR and LEET $B \rightarrow K_2^*$ transition form factors [42, 54], for different New Physics scenarios.[31]

ues close to its SM value as can be seen from Fig2. The optimized angular observable P_1 gives an enhancement about 10% – 15% in all the NP scenarios for low q^2 bin by SM predictions. S1 and S3 speculate positive values for P_2 , S2 scenario suggests a negative value for P_2 . Whereas SM suggests comparatively larger negative val-

ues. Therefore, precise measurement of q^2 distribution of P_2 within a low q^2 region could serve to distinguish S2 from the other two scenarios. This can also be seen from Fig.3. In the presence of NP zero crossing point for P_2 shifts towards higher q^2 as can be seen from Fig.3. The predictions for the optimized angular observable P_2 are shown in the top right panel of Fig3 shows enhancement from SM predictions for low q^2 . However, there is no meaningful deviation from the SM in the observable P'_4 for all the NP scenarios under consideration. This can be seen in Fig 3, that the maximum and minimum possible values of observable P'_4 in all the NP scenarios overlap with the SM band shown in color cyan. The optimized observable P'_5 shows enhancement from the corresponding SM values in all universal NP scenarios, and the zero crossing point shifts towards high q^2 in the presence of NP, S2 scenario gives an enhancement of about 22% whereas in S3 scenario enhancement is almost 42% in low q^2 bin. Nevertheless, S1 scenario shows nearly two-fold enhancement from SM predictions in the low q^2 bin which makes P'_5 a valuable observable to study NP effects. From the bottom right panel of Fig 3 it can be observed that NP enhance optimized observable P'_5 from its SM prediction for $1 \text{ GeV}^2 \leq q^2 \leq 6 \text{ GeV}^2$. Similar to A_{FB} , we calculated P_2 and P'_5 for $q^2 < q_0^2$ and $q_0^2 > q^2$ as depicted in TableIII.

Observable	Solutions	q^2 Range	Predictions
A_{FB}	SM	$[q_{min}^2 - 2.8]$	0.034 ± 0.012
		$[2.8 - q_{max}^2]$	-0.043 ± 0.014
	S1	$[q_{min}^2 - 3.65]$	0.043 ± 0.015
		$[3.65 - q_{max}^2]$	-0.030 ± 0.015
	S2	$[q_{min}^2 - 3.13]$	0.038 ± 0.013
		$[3.13 - q_{max}^2]$	-0.039 ± 0.015
S3	$[q_{min}^2 - 3.44]$	0.047 ± 0.015	
	$[3.44 - q_{max}^2]$	-0.038 ± 0.017	
P'_5	SM	$[q_{min}^2 - 1.8]$	0.511 ± 0.099
		$[1.8 - q_{max}^2]$	-0.458 ± 0.133
	S1	$[q_{min}^2 - 2.42]$	0.545 ± 0.108
		$[2.42 - q_{max}^2]$	-0.323 ± 0.127
	S2	$[q_{min}^2 - 2.04]$	0.515 ± 0.099
		$[2.04 - q_{max}^2]$	-0.425 ± 0.139
S3	$[q_{min}^2 - 2.29]$	0.578 ± 0.117	
	$[2.29 - q_{max}^2]$	-0.390 ± 0.138	
P_2	SM	$[q_{min}^2 - 2.81]$	0.213 ± 0.008
		$[2.81 - q_{max}^2]$	-0.258 ± 0.065
	S1	$[q_{min}^2 - 3.67]$	0.094 ± 0.053
		$[3.67 - q_{max}^2]$	0.222 ± 0.015
	S2	$[q_{min}^2 - 3.15]$	0.206 ± 0.009
		$[3.15 - q_{max}^2]$	-0.230 ± 0.072
S3	$[q_{min}^2 - 3.47]$	0.218 ± 0.015	
	$[3.47 - q_{max}^2]$	-0.180 ± 0.072	

TABLE III: Predictions for forward-backward asymmetry (A_{FB}) and optimized observable P'_5 and P_2 , on both side of their zero crossing value for $B \rightarrow K_2^*(\rightarrow K\pi)\mu^+\mu^-$ decay, here $q_{min}^2 = 4m_\mu^2$ and $q_{max}^2 = 6 \text{ GeV}^2$.

VI. Z' MODEL

In this section, we study $B \rightarrow K_2^*(1430)\mu^+\mu^-$ decay in a non-universal Z' model, where Z' adheres additional $U(1)'$ symmetry. In the presence of Z' , the FCNC process $b \rightarrow s\mu^+\mu^-$ accomplished at tree level. It couples to left and right-handed muons exclusively without interacting with leptons belonging to other generations. Furthermore, it couples to both left and right-handed quarks. Flavor-changing interaction for $b \rightarrow s\mu^+\mu^-$ transition in

Z' model is given by [78]:

$$\begin{aligned} L_{Z'} &\supset J^\alpha Z'_\alpha \\ J^\alpha &\supset g_L^{bs} \bar{s} \gamma^\alpha P_L b + g_L^{\mu\mu} \bar{\mu} \gamma^\alpha P_L \mu + h.c. \end{aligned} \quad (18)$$

$$\begin{aligned} \mathcal{H}_{eff}^{Z'} &\supset \frac{g_L^{bs}}{M_{Z'}^2} (\bar{s} \gamma^\alpha P_L b) [\bar{\mu} \gamma_\alpha (g_L^{\mu\mu} P_L + g_R^{\mu\mu} P_R) \mu] + \frac{g_R^{bs}}{M_{Z'}^2} (\bar{s} \gamma^\alpha P_R b) [\bar{\mu} \gamma_\alpha (g_L^{\mu\mu} P_L + g_R^{\mu\mu} P_R) \mu] \\ &+ \frac{(g_L^{bs})^2}{2M_{Z'}^2} (\bar{s} \gamma^\alpha P_L b) (\bar{s} \gamma_\alpha P_L b) + \frac{(g_R^{bs})^2}{2M_{Z'}^2} (\bar{s} \gamma^\alpha P_R b) (\bar{s} \gamma_\alpha P_R b) \\ &+ \frac{(g_L^{bs} g_R^{bs})}{M_{Z'}^2} (\bar{s} \gamma^\alpha P_L b) (\bar{s} \gamma_\alpha P_R b). \end{aligned} \quad (19)$$

In Eqn. 19 initial two terms correspond to $b \rightarrow s\mu^+\mu^-$ transition and the rest terms induce $B_s - \bar{B}_s$ mixing. In the presence of Z' the Wilson coefficients in $b \rightarrow s\mu^+\mu^-$ transition get modified as:

$$C_{9,10} = C_{9,10}^{SM} + C_{9,10}^{NP} \quad (20)$$

after matching with eqn. 2 we get,

$$\begin{aligned} C_9^{NP} &= \frac{-N_1}{2} g_L^{bs} (g_L^{\mu\mu} + g_R^{\mu\mu}) \\ C_{10}^{NP} &= \frac{N_1}{2} g_L^{bs} (g_L^{\mu\mu} - g_R^{\mu\mu}). \end{aligned} \quad (21)$$

The right-handed quark coupling influences chirally flipped Wilson coefficients $C'_{9,10}$, as:

$$\begin{aligned} C'_9 &= \frac{-N_1}{2} g_R^{bs} (g_L^{\mu\mu} + g_R^{\mu\mu}) \\ C'_{10} &= \frac{N_1}{2} g_R^{bs} (g_L^{\mu\mu} - g_R^{\mu\mu}). \end{aligned} \quad (22)$$

Where $N_1 = \sqrt{2}\pi/(\alpha_{em} V_{tb} V_{ts}^* M_{Z'}^2)$. It is evident from universal $b \rightarrow sll$ fitting that $C_9^{NP} < 0$, $C_9^{NP} = -C_{10}^{NP}$ and $C_9^{NP} = -C'_{9,10}$ generates a good fit to data [31]. It can be seen from Eqn. 21 that right handed quark coupling (g_R^{bs}) do not contribute in C_9^{NP} and C_{10}^{NP} . S1

Here $g_{L,R}^{\mu\mu}$ and $g_{L,R}^{bs}$ are left and right-handed coupling of Z' boson with muons and quarks respectively. After integrating out heavy Z' we get an effective four-fermion Hamiltonian which not only induces $b \rightarrow s\mu\mu$ transition but also generates $B_s - \bar{B}_s$ mixing. The relevant effective Hamiltonian can be written as [79, 80]:

NP scenario can be achieved by substituting $g_L^{\mu\mu} = g_R^{\mu\mu}$ along with $g_R^{bs} = 0$. While the S2 NP scenario can be obtained using $g_R^{\mu\mu} = g_R^{bs} = 0$. However, the S3 NP scenario can be induced by using $g_L^{\mu\mu} = g_R^{\mu\mu}$, and $g_L^{bs} = g_R^{bs}$. We now proceed to discuss $B_s - \bar{B}_s$ mixing. The NP effective Hamiltonian for $B_s - \bar{B}_s$ mixing can be described as:

$$\begin{aligned} \mathcal{H}^{\Delta B=2} &\supset \frac{4G_f}{\sqrt{2}} (V_{tb} V_{ts}^*) [C_1^{bs} (\bar{s} \gamma^\alpha P_L b)^2 + C_2^{bs} (\bar{s} \gamma^\alpha P_R b)^2 \\ &+ C_3^{bs} (\bar{s} \gamma^\alpha P_L b) (\bar{s} \gamma_\alpha P_R b)]. \end{aligned} \quad (23)$$

after matching with eqn.19 NP Wilson coefficients are given as:

$$\begin{aligned} C_1^{bs} &= \frac{1}{4\sqrt{2}G_f M_{Z'}^2} \left(\frac{g_L^{bs}}{V_{tb} V_{ts}^*} \right)^2 \\ C_2^{bs} &= \frac{1}{4\sqrt{2}G_f M_{Z'}^2} \left(\frac{g_R^{bs}}{V_{tb} V_{ts}^*} \right)^2 \\ C_3^{bs} &= \frac{1}{4\sqrt{2}G_f M_{Z'}^2} \left(\frac{g_L^{bs} g_R^{bs}}{(V_{tb} V_{ts}^*)^2} \right). \end{aligned} \quad (24)$$

Neglecting scalar and tensor operators, which are currently disfavored by $b \rightarrow s$ data, the contribution to $B_s - \bar{B}_s$ mixing normalized to the Standard Model is represented by

$$\begin{aligned} \frac{\Delta M_s^{SM+NP}}{\Delta M_s} &= \left| 1 + \frac{\eta^{6/23}}{R_{loop}^{SM}} [C_1^{bs} + C_2^{bs} \right. \\ &\left. - \frac{C_3}{2\eta^{3/23}} \left(\frac{B_5}{B_1} \left(\frac{M_{B_s}^2}{(m_b + m_s)^2} + \frac{3}{2} \right) + \frac{B_4}{B_1} \left(\frac{M_{B_s}^2}{(m_b + m_s)^2} + \frac{1}{6} \right) (\eta^{-27/23} - 1) \right) \right|. \end{aligned} \quad (25)$$

In the above eqn. 25, $\eta = \alpha_s(\mu_{NP})/\alpha_s(m_b)$, SM loop

function, $R_{loop}^{SM} = 1.310 \pm 0.010$ [81] and the Bag param-

eters B_i , ($i = 1, 4, 5$) are defined in [81]. Using eqn. 23 and 24, we get:

$$\frac{\Delta M_s^{SM+Z'}}{\Delta M_s} \approx |1 + 5 \times 10^3 \{(g_L^{bs})^2 + (g_R^{bs})^2 - 9(g_L^{bs}g_R^{bs})\}|.$$

The mass of the Z' is significantly higher than the electroweak scale implying that Z' coupling must adhere to $SU(2)_L$ gauge invariance. As a consequence of this Z' interacts with the left-handed neutrinos through the $g_L^{\mu\mu}$ coupling. This interaction introduces an additional term in the effective Hamiltonian which can be represented as:

$$\mathcal{H}_{eff}^{Z'} \supset \frac{g_L^{\mu\mu}}{M_{Z'}^2} (\bar{\nu}_\mu \gamma^\alpha P_L \nu_\mu) [\bar{\mu} \gamma_\alpha (g_L^{\mu\mu} P_L + g_R^{\mu\mu} P_R) \mu]. \quad (26)$$

The aforementioned term plays a role in influencing neutrino trident production ($\nu N \rightarrow \nu N \mu^+ \mu^-$) and modifies the cross-section as:

$$\begin{aligned} R_\nu &= \frac{\sigma}{\sigma_{SM}} \quad (27) \\ &= \frac{1}{1 + (1 + 4s_W^2)^2} \left[\left(1 + \frac{\nu^2 g_L^{\mu\mu} (g_L^{\mu\mu} - g_R^{\mu\mu})}{M_{Z'}^2} \right)^2 \right. \\ &\quad \left. + \left(1 + 4s_W^2 + \frac{\nu^2 g_L^{\mu\mu} (g_L^{\mu\mu} + g_R^{\mu\mu})}{M_{Z'}^2} \right)^2 \right] \quad (28) \end{aligned}$$

Here $\nu = 246$ GeV and $s_W = \sin \theta_W$. Neutrino trident impose constraints on individual muon coupling $g_{L,(R)}^{\mu\mu}$, experimental measurement for this is 0.82 ± 0.28 . We perform χ^2 analysis to find the NP parameter space allowed by the current flavor data.

$$\chi^2(g_{L,R}^{bs}, g_{L,R}^{\mu\mu}) = \sum_K \frac{\mathcal{O}_K^{theory}(g_{L,R}^{bs}, g_{L,R}^{\mu\mu}) - \mathcal{O}_K^{exp}}{\sigma_{total,K}^2} \quad (29)$$

where \mathcal{O}_K^{theory} is the theoretical prediction, \mathcal{O}_K^{exp} is the experimental central value and $\sigma_{total,K}$ is the total uncertainty. To calculate χ^2 fit we used constraints from a global fit to all $b \rightarrow sl^+l^-$ observables for various NP scenarios as described in Table I. Contribution of $B_s - \bar{B}_s$ mixing in χ^2 is given as:

$$\chi_{\Delta M_s}^2 = \left(\frac{((g_L^{bs})^2 + (g_R^{bs})^2 - 9g_L^{bs}g_R^{bs}) - 7.69 \times 10^{-6}}{12.94 \times 10^{-6}} \right)^2 \quad (30)$$

Where we have used $\Delta M_s^{SM}/\Delta M_s^{exp} = 1.04_{-0.07}^{+0.04}$ [81]. The neutrino trident contribution to χ^2 is given by:

$$\chi_{trident}^2 = \left(\frac{R_\nu - 0.82}{0.28} \right)^2 \quad (31)$$

The experimental value of R_ν is 0.82 ± 0.28 [82] and the theoretical expression of R_ν is given by eqn. 28. The total χ^2 will be:

$$\chi_{total}^2 = \chi_{b \rightarrow sl}^2 + \chi_{\Delta M_s}^2 + \chi_{trident}^2 \quad (32)$$

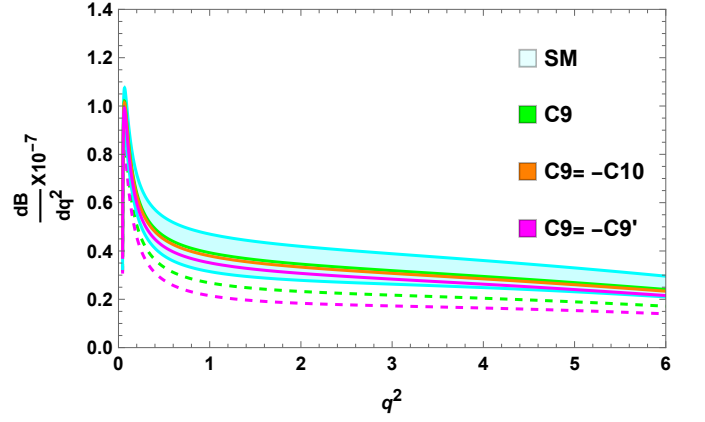


FIG. 4: Plots for q^2 distribution in SM and Z' model along with new physics scenarios for branching ratio of $B \rightarrow K_2^*(\rightarrow K\pi)\mu^+\mu^-$ decay.

The permissible new physics couplings are determined by minimizing the χ^2 function. To perform this minimization we used the CERN minimization code MINUIT [84].

The best-fit values of coupling parameters ($g_{L,R}^{\mu\mu}$, $g_{L,R}^{bs}$) associated with the 1TeV Z' model are given in TableIV. Comparing these results with NP Wilson coefficients, TableI, we see that Wilson coefficients within Z' model are consistent with NP Wilson coefficients. The q^2 dependency for differential branching ratio $\frac{dB}{dq^2}$ in SM along with three NP scenarios in Z' are shown in Fig 4. It is lucient from Fig 4 that there is suppression in $\frac{dB}{dq^2}$ in Z' over the SM. Furthermore, the maximal suppression from SM is about $\sim 28\%$ for Z3 scenario. From both Longitudinal Polarization plot and Table(V), it is evident that none of the NP scenarios in Z' shows a significant deviation from SM value in the low q^2 bin. Similarly, no remarkable deviation over SM is observed for optimized observable P_4' in the Z' model. All three scenarios in Z' model manifest enhancement in optimized observable P_1 by $10 \sim 20\%$ over SM predictions, and maximum enhancement for Z1 scenario in low q^2 bin. In the right pannel of Fig 5, the q^2 dependency of A_{FB} intimates zero crossing is positive to negative, and zero crossing shifted toward higher q^2 than SM value. The prediction of A_{FB} in heavy Z' shows enhancement from SM value. It is apparent from Fig 4, that there is a finite enhancement in P_5' in Z' over SM for all scenarios. It leads to maximum enhancement about twofold for Z1 scenario whereas, almost 22% and 42% for Z2 and Z3 scenario for low q^2 bin. Enhancement in P_5' in Z' over SM makes it a useful observable in low q^2 bin.

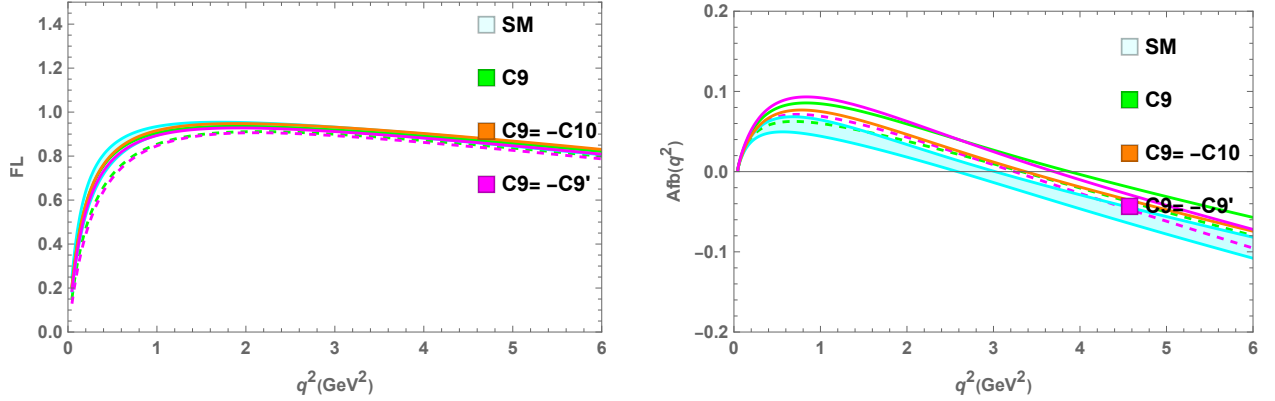
VII. CONCLUSION

In this work, we study several observables for $B \rightarrow K_2^*(\rightarrow K\pi)\mu^+\mu^-$ decay in SM, and NP scenarios, under the assumptions that new physics couplings are real

Scenario	Couplings	Wilson Coefficients
Z1: C_9^{NP}	$g_R^{bs} = 0, g_L^{bs} = 0.00285,$ $g_L^{\mu\mu} = g_R^{\mu\mu} = -0.2986$	$C_9^{NP} = -N_1 g_L^{bs} g_L^{\mu\mu}$
Z2: $C_9^{NP} = -C_{10}^{NP}$	$g_R^{bs} = 0, g_L^{\mu\mu} = -0.2782,$ $g_R^{\mu\mu} = 0, g_L^{bs} = 0.00283$	$C_9^{NP} = -(N_1/2) g_L^{bs} g_L^{\mu\mu}$
Z3: $C_9^{NP} = -C_9'$	$g_L^{\mu\mu} = -0.7125, g_R^{\mu\mu} = -0.712,$ $g_L^{bs} = -g_R^{bs} = 0.0096$	$C_9^{NP} = -(N_1/2) g_L^{bs} (g_L^{\mu\mu} + g_R^{\mu\mu})$

TABLE IV: Universal 1D favored NP scenarios that can be generated in Z' model

Angular Observable	Form factor	SM	Z1	Z2	Z3
$BR \times 10^7$	LCSR	1.554 ± 0.559	1.2805 ± 0.449	1.231 ± 0.444	1.149 ± 0.394
	LEET	1.212 ± 0.605	1.084 ± 0.538	1.022 ± 0.512	0.991 ± 0.488
F_L	LCSR	0.835 ± 0.016	0.822 ± 0.020	0.8336 ± 0.0169	0.812 ± 0.023
	LEET	0.721 ± 0.105	0.700 ± 0.113	0.724 ± 0.104	0.667 ± 0.121
A_{FB}	LCSR	-0.015 ± 0.011	0.0075 ± 0.014	-0.0057 ± 0.013	0.00346 ± 0.015
	LEET	-0.050 ± 0.026	0.0 ± 0.001	-0.028 ± 0.015	-0.008 ± 0.004
P_1	LCSR	-0.446 ± 0.149	-0.3916 ± 0.142	-0.412 ± 0.146	-0.406 ± 0.136
	LEET	0.374 ± 0.001	0.009 ± 0.001	0.225 ± 0.001	0.008 ± 0.001
P_2	LCSR	-0.112 ± 0.086	0.048 ± 0.085	-0.042 ± 0.094	0.0205 ± 0.088
	LEET	-0.171 ± 0.001	0.008 ± 0.001	-0.093 ± 0.003	-0.023 ± 0.002
P_4'	LCSR	0.975 ± 0.111	0.935 ± 0.110	0.923 ± 0.125	0.932 ± 0.104
	LEET	0.879 ± 0.010	0.840 ± 0.011	0.823 ± 0.0165	0.832 ± 0.012
P_5'	LCSR	-0.349 ± 0.137	-0.149 ± 0.133	-0.277 ± 0.143	-0.206 ± 0.145
	LEET	-0.548 ± 0.0032	-0.315 ± 0.001	-0.473 ± 0.002	-0.389 ± 0.0007

TABLE V: Angular Observables SM and Z' predictions with 1σ for q^2 [1-6] GeV^2 bin following LCSR and LEET $B \rightarrow K_2^*$ transition form factors [42, 54], for different New Physics scenarios.FIG. 5: Same as for Fig. 4 except for F_L and A_{FB} observables.

and universal in $b \rightarrow sl^+l^-$ ($l = e, \mu, \tau$) transition. Firstly, we obtained four-fold angular distribution for $B \rightarrow K_2^*(\rightarrow K\pi)l^+l^-$ for vector, axial vector, scalar, and pseudo-scalar interaction, we scrutinize the demeanor of differential branching ratio, forward-backward asymmetry A_{FB} , longitudinal polarization asymmetry F_L and optimized observables P_i' in SM and NP scenarios. We explored the above observables by considering all form factors procured through the light cone sum rule and large energy effective theory.

Our analysis revealed that there is a depletion in the branching ratio in NP as compared to SM. It is $\sim 15\%$ for

S1, and up to $\sim 25\%$ for S2, and S3 NP scenarios. NP solutions provide finite enhancement in muon forward-backward asymmetry (A_{FB}). On the other hand, longitudinal fraction (F_L) shows no significant deviations with SM value. We also studied optimized observables P_i' and observed that there is significant deviations from SM contribution.

We then consider TeV range non-universal Z' model which can generate 1D favored solutions. The presence of $B_s - \bar{B}_s$ mixing and neutrino trident impose extra constraints on Z' coupling. Using the above constraints, we perform a global fit to determine Z' couplings ($g_{L,R}^{bs}$,

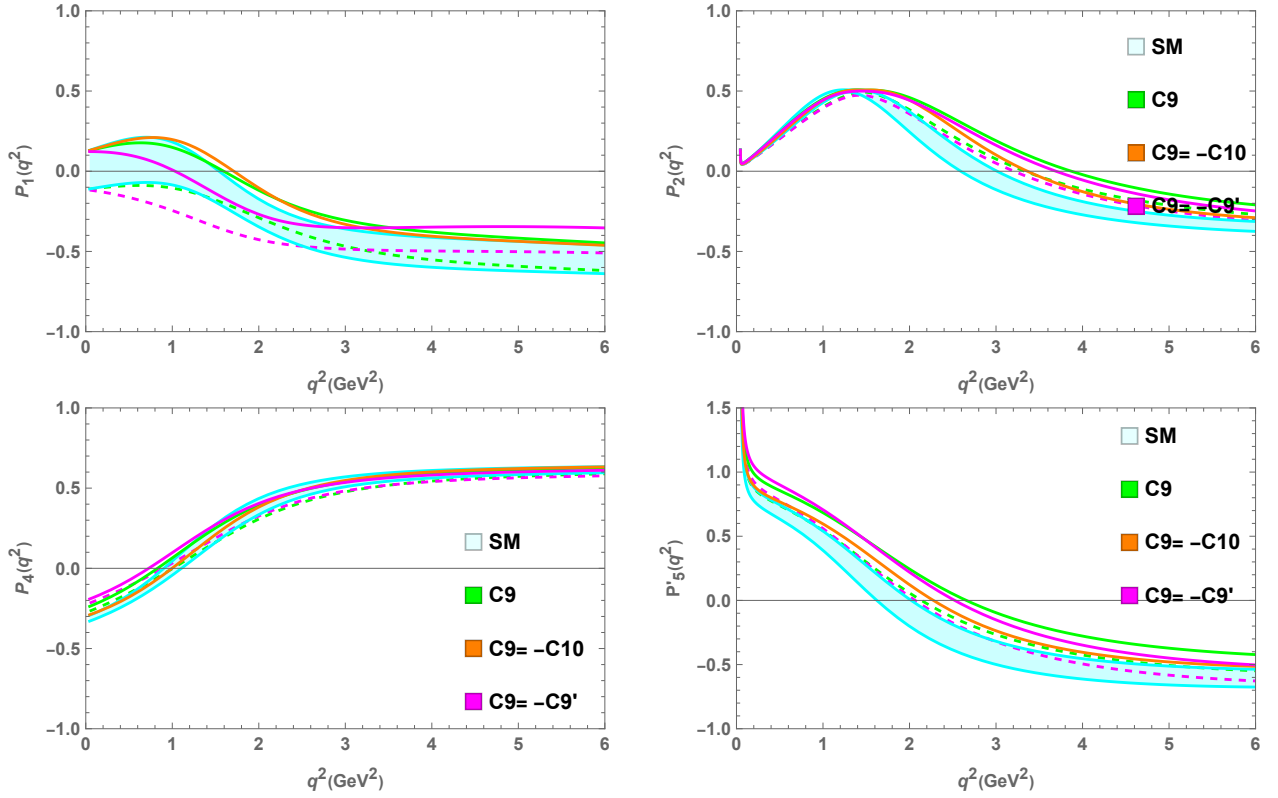


FIG. 6: Same as for Fig. 4 except for optimized observables P'_i .

$g_{L,R}^{\mu\mu}$), and Wilson coefficients. We observed that Wilson coefficients under 1TeV Z' model are consistent with new physics Wilson coefficients. We conclude this model does not have any additional advantage over new physics in resolving $b \rightarrow s\mu^+\mu^-$ anomalies.

VIII. APPENDIX

A. Effective Wilson Coefficient for $b \rightarrow sl^+l^-$ transition

The effective Wilson coefficients for $b \rightarrow sll$ transition can be written as describe in [56]:

$$\begin{aligned}
 C_7^{eff} &= C_7 - C_5/3 - C_6 \\
 C_9^{eff}(q^2) &= C_9(\mu) + h(\hat{m}_c, \hat{s})C_0 - \frac{1}{2}h(1, \hat{s})(4C_3 + 4C_4 \\
 &\quad + 3C_5 + C_6) - \frac{1}{2}h(0, \hat{s})(C_3 + 3C_4) \\
 &\quad + \frac{2}{9}(3C_3 + C_4 + 3C_5 + C_6)
 \end{aligned} \tag{33}$$

With $\hat{s} = q^2/m_b^2$, $C_0 = C_1 + 3C_2 + 3C_3 + C_4 + 3C_5 + C_6$ and $\hat{m}_c = m_c/m_b$

The auxiliary functions used as :
if $x = 4z^2/s < 1$

$$\begin{aligned}
 h(z, \hat{s}) &= -\frac{8}{9} \ln \frac{m_b}{\mu} - \frac{8}{9} \ln z + \frac{8}{27} + \frac{4x}{9} - \\
 &\quad \frac{2}{9}(2+x)|1-x|^{1/2} \ln |\sqrt{1-x} + 1/\sqrt{1-x} - 1| - i\pi
 \end{aligned}$$

$$\begin{aligned}
 h(z, \hat{s}) &= -\frac{8}{9} \ln \frac{m_b}{\mu} - \frac{8}{9} \ln z + \frac{8}{27} + \frac{4x}{9} \\
 &\quad - \frac{2(2+x)}{9}|1-x|^{1/2} * 2 \arctan \frac{1}{\sqrt{x-1}}, x = \frac{4z^2}{s} > 1
 \end{aligned}$$

$$h(0, \hat{s}) = -\frac{8}{9} \ln \frac{m_b}{\mu} - \frac{4 \ln \hat{s}}{9} + \frac{8}{27} + \frac{4i\pi}{9} \tag{34}$$

B. Angular Coefficient

The vector and axial-vector transversity amplitudes can be expressed as:

$$\begin{aligned}
A_{0L,R} &= N \frac{\sqrt{\lambda}}{\sqrt{6}m_B m_{K_2^*}} \frac{1}{2m_{K_2^*} \sqrt{q^2}} [(C_{9-} \mp C_{10-}) \\
&\quad ((m_B^2 - m_{K_2^*}^2 - q^2)(m_B + m_{K_2^*})A_1 \\
&\quad - \frac{\lambda}{m_B + m_{K_2^*}} A_2) + 2m_b C_7 ((m_B^2 + 3m_{K_2^*}^2 - q^2)T_2 \\
&\quad - \frac{\lambda}{m_B^2 - m_{K_2^*}^2} T_3)], \\
A_{\perp L,R} &= -\sqrt{2}N \frac{\sqrt{\lambda}}{\sqrt{8}m_B m_{K_2^*}} [(C_{9+} \mp C_{10+}) \frac{\sqrt{\lambda}V}{m_B + m_{K_2^*}} \\
&\quad + \frac{2m_b C_7}{q^2} \sqrt{\lambda} T_1], \\
A_{\parallel L,R} &= \sqrt{2}N \frac{\sqrt{\lambda}}{\sqrt{8}m_B m_{K_2^*}} [(C_{9-} \mp C_{10-})(m_B + m_{K_2^*})A_1 \\
&\quad + \frac{2m_b C_7}{q^2} (m_B^2 - m_{K_2^*}^2)T_2], \\
A_t &= N \frac{\lambda}{\sqrt{q^2} \sqrt{6}m_B m_{K_2^*}} \left[2C_{10-} + \frac{q^2}{m_l} (C_P - C'_P) \right] A_0, \tag{35}
\end{aligned}$$

where $C_{9\pm} = (C_9 \pm C'_9)$, and $C_{10\pm} = (C_{10} \pm C'_{10})$. The transversity amplitudes for scalar interactions can be written as

$$A_S = 2N\sqrt{\lambda} \frac{\sqrt{\lambda}}{\sqrt{6}m_B m_{K_2^*}} \left[\frac{(C_S - C'_{S'})}{(m_b + m_s)} A_0 \right], \tag{36}$$

where $\lambda = m_B^4 + m_{K_2^*}^4 + q^4 - 2(m_B^2 m_{K_2^*}^2 + m_B^2 q^2 + m_{K_2^*}^2 q^2)$ and normalization constant is given by

$$\begin{aligned}
N &= \left[\frac{G_F^2 \alpha_e^2}{3 \cdot 2^{10} \pi^5 m_B^3} |V_{tb} V_{ts}^*|^2 \lambda^{1/2} (m_B^2, m_{K_2^*}^2, q^2) \mathcal{B}(K_2^* \rightarrow K\pi) \beta_\ell \right]^{\frac{1}{2}} \\
\beta_\ell &= \sqrt{1 - \frac{4m_\ell^2}{q^2}}. \tag{37}
\end{aligned}$$

IX. ACKNOWLEDGMENTS

We thank Dinesh Kumar, Suman Kumbhakar, A. K. Alok and N. R. S. Chundawat for useful discussions. RS acknowledges the financial support from

the Science and Engineering Research Board (SERB) for the National PostDoctoral Fellowship (file no. NPDF/PDF/2021/003328).

Input Parameters	Numeric Value
m_B	5.279 GeV
$m_{K_2^*}$	1.4324 ± 1.3 GeV
m_b^{pole}	4.7417 GeV
m_c^{pole}	1.5953 GeV
$ V_{ts}^* V_{tb} $	0.04088 ± 0.00055
G_F	1.1663787×10^{-5}
α_e	1/133.28
τ_{B_s}	1.638×10^{-12}
$\text{Br}(K_2^* \rightarrow K\pi)$	$(49.4 \pm 1.2)\%$

TABLE VI: The numerical inputs used in our analysis [85, 86].

F	$F^{B(s)K_2^*}(0)$	$a_{K_2^*}$	$b_{K_2^*}$
V	0.16 ± 0.02	2.08	1.50
A_0	0.25 ± 0.04	1.57	0.10
A_1	0.14 ± 0.02	1.23	0.49
A_2	0.05 ± 0.02	1.32	14.9
T_1	0.14 ± 0.02	2.07	1.50
T_2	0.14 ± 0.02	1.22	0.35
T_3	$0.01_{-0.01}^{+0.02}$	9.91	276

TABLE VII: The relevant form factors parameters [42]

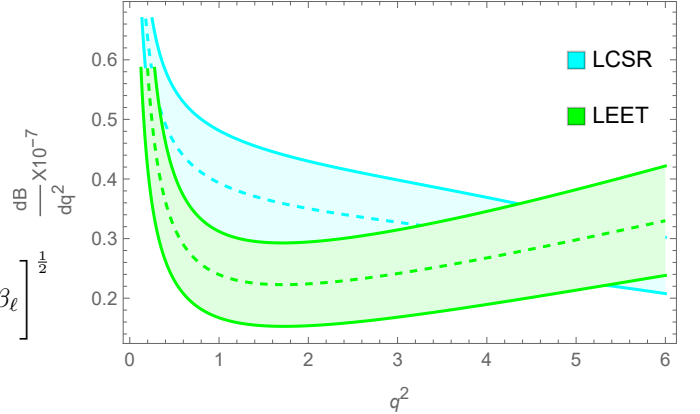


FIG. 7: Plot for q^2 distribution in SM for branching ratio of $B \rightarrow K_2^*(\rightarrow K\pi)\mu^+\mu^-$ decay using LCSR and LEET form factor formulation. The solid lines represent the maximum and minimum boundaries for each form factor formulation and dotted lines present central values.

-
- [1] R. Fleischer, E. Malami, A. Rehult and K. K. Vos, [arXiv:2404.07588 [hep-ph]].
- [2] R. Fleischer, E. Malami, A. Rehult and K. K. Vos, *JHEP* **03**, 113 (2023) [arXiv:2212.09575 [hep-ph]].
- [3] N. R. Singh Chundawat, *Phys. Rev. D* **107** (2023) no.7, 075014 [arXiv:2207.10613 [hep-ph]].
- [4] S. N. Gangal, [arXiv:2209.02476 [hep-ph]].
- [5] D. Das, J. Das, G. Kumar and N. Sahoo, *Phys. Rev. D* **108**, no.1, 1 (2023) [arXiv:2211.09065 [hep-ph]].
- [6] A. K. Alok, S. Banerjee, N. R. S. Chundawat and S. U. Sankar, *JHEP* **05**, 124 (2024) [arXiv:2402.02470 [hep-ph]].
- [7] R. Aaij *et al.* [LHCb Collaboration], *JHEP* **1509**, 179 (2015) [arXiv:1506.08777 [hep-ex]].
- [8] R. Aaij *et al.* [LHCb], *Phys. Rev. Lett.* **127** (2021) no.15, 151801 [arXiv:2105.14007 [hep-ex]].
- [9] R. Aaij *et al.* [LHCb Collaboration], *Phys. Rev. Lett.* **111**, 191801 (2013) [arXiv:1308.1707 [hep-ex]].
- [10] R. Aaij *et al.* [LHCb Collaboration], *JHEP* **1602**, 104 (2016) [arXiv:1512.04442 [hep-ex]].
- [11] R. Aaij *et al.* [LHCb], *Phys. Rev. Lett.* **125** (2020) no.1, 011802 [arXiv:2003.04831 [hep-ex]].
- [12] S. Descotes-Genon, T. Hurth, J. Matias and J. Virto, *JHEP* **1305**, 137 (2013) [arXiv:1303.5794 [hep-ph]].
- [13] R. Aaij *et al.* [LHCb], *Phys. Rev. Lett.* **131**, no.5, 051803 (2023) [arXiv:2212.09152 [hep-ex]].
- [14] R. Aaij *et al.* [LHCb], *Phys. Rev. Lett.* **108**, no.3, 032002 (2023) [arXiv:2212.09153 [hep-ex]].
- [15] A. K. Alok, A. Datta, A. Dighe, M. Duraisamy, D. Ghosh and D. London, *JHEP* **1111**, 121 (2011) [arXiv:1008.2367 [hep-ph]].
- [16] A. K. Alok, A. Datta, A. Dighe, M. Duraisamy, D. Ghosh and D. London, *JHEP* **1111**, 122 (2011) [arXiv:1103.5344 [hep-ph]].
- [17] S. Descotes-Genon, J. Matias and J. Virto, *Phys. Rev. D* **88**, 074002 (2013) [arXiv:1307.5683 [hep-ph]].
- [18] W. Altmannshofer and D. M. Straub, *Eur. Phys. J. C* **73**, 2646 (2013) [arXiv:1308.1501 [hep-ph]].
- [19] T. Hurth and F. Mahmoudi, *JHEP* **04** (2014), 097 [arXiv:1312.5267 [hep-ph]].
- [20] A. Datta, J. Kumar and D. London, *Phys. Lett. B* **797**, 134858 (2019) [arXiv:1903.10086 [hep-ph]].
- [21] J. Kumar and D. London, *Phys. Rev. D* **99**, no.7, 073008 (2019) [arXiv:1901.04516 [hep-ph]].
- [22] A. K. Alok, A. Dighe, S. Gangal and D. Kumar, *JHEP* **06** (2019), 089 [arXiv:1903.09617 [hep-ph]].
- [23] A. Carvunis, F. Dettori, S. Gangal, D. Guadagnoli and C. Normand, [arXiv:2102.13390 [hep-ph]].
- [24] M. Algueró, B. Capdevila, S. Descotes-Genon, J. Matias and M. Novoa-Brunet, [arXiv:2104.08921 [hep-ph]].
- [25] L. S. Geng, B. Grinstein, S. Jäger, S. Y. Li, J. Martin Camalich and R. X. Shi, [arXiv:2103.12738 [hep-ph]].
- [26] T. Hurth, F. Mahmoudi, D. M. Santos and S. Neshatpour, [arXiv:2104.10058 [hep-ph]].
- [27] A. Angelescu, D. Bečirević, D. A. Faroughy, F. Jaffredo and O. Sumensari, *Phys. Rev. D* **104**, no.5, 055017 (2021) [arXiv:2103.12504 [hep-ph]].
- [28] A. K. Alok, N. R. Singh Chundawat, S. Gangal and D. Kumar, *Eur. Phys. J. C* **82**, no.10, 967 (2022) [arXiv:2203.13217 [hep-ph]].
- [29] M. Ciuchini, M. Fedele, E. Franco, A. Paul, L. Silvestrini and M. Valli, *Phys. Rev. D* **107** (2023) no.5, 055036 [arXiv:2212.10516 [hep-ph]].
- [30] N. R. Singh Chundawat, *Phys. Rev. D* **107** (2023) no.5, 055004 [arXiv:2212.01229 [hep-ph]].
- [31] A. K. Alok, N. R. Singh Chundawat and A. Mandal, *Phys. Lett. B* **847**, 138289 (2023) [arXiv:2303.16606 [hep-ph]].
- [32] A. K. Alok, N. R. S. Chundawat, J. Kumar, A. Mandal and U. Tamponi, [arXiv:2405.18488 [hep-ph]].
- [33] M. Algueró, A. Biswas, B. Capdevila, S. Descotes-Genon, J. Matias and M. Novoa-Brunet, [arXiv:2304.07330 [hep-ph]].
- [34] W. Altmannshofer and P. Stangl, [arXiv:2103.13370 [hep-ph]].
- [35] T. Hurth, F. Mahmoudi and S. Neshatpour, [arXiv:2310.05585 [hep-ph]].
- [36] S. Nishida *et al.*, Radiative B meson decays into K pi gamma and K pi pi gamma final states, *Phys. Rev. Lett.* **89** (2002) 231801, [arXiv:0205025 [hep-ex]].
- [37] B. Aubert *et al.*, *Phys. Rev. D* **70** (2004) 091105 [arXiv:0409035 [hep-ex]].
- [38] Isgur, N. Scora, D. Grinstein, B., and Wise M. B, *Phys. Rev. D* **39(3)**, 799–818 (1989).
- [39] D. Scora and N. Isgur *Phys. Rev. D* **52**, 2783–2812 (1995), [arXiv:hep-ph/9503486 [hep-ph]].
- [40] N. Sharma and R. C. Verma, *Phys. Rev. D* **82**, 094014 (2010) [arXiv:1004.1928 [hep-ph]].
- [41] Wei. Wang *Phys. Rev. D* **83**, 014008 (2011) [arXiv:1008.5326 [hep-ph]].
- [42] K. C. Yang *Phys. Lett. B* **695**, 444–448 (2011) [arXiv:1010.2944 [hep-ph]].
- [43] J. Charles, A. Le Yaouanc, L. Oliver, O. Pene, and J. C. Raynal *Phys. Rev. D* **60**, 014001 (1990) [arXiv:9812358 [hep-ph]].
- [44] N. Katirci and K. Azizi, *JHEP* **07**, (2011) 043 [arXiv:1105.3636 [hep-ph]].
- [45] S. Kumbhakar, R. Sain and J. Vardani, *J. Phys. G* **50**, no.9, 095003 (2023), doi:10.1088/1361-6471/ace923, [arXiv:2208.05923 [hep-ph]].
- [46] I. Ahmed, M. J. Aslam, M. Junaid, and S. Shafaq, *JHEP* **02**, (2012) 045
- [47] S. Rai Choudhury, A. S. Cornell, G. C. Joshi and B. H. J. McKellar, *Phys. Rev. D* **74**, 054031 (2006) [arXiv:hep-ph/0607289 [hep-ph]].
- [48] M. Junaid, M. J. Aslam and I. Ahmed, *Int. J. Mod. Phys. A* **27**, 1250149 (2012) [arXiv:1103.3934 [hep-ph]].
- [49] M. K. Mohapatra and A. Giri, *Phys. Rev. D* **104**, no.9, 095012 (2021) [arXiv:2109.12382 [hep-ph]].
- [50] R. H. Li, C. D. Lu and W. Wang, *Phys. Rev. D* **83** (2011), 034034 [arXiv:1012.2129 [hep-ph]].
- [51] T. M. Aliev and M. Savci, *Phys. Rev. D* **85**, 015007 (2012) [arXiv:1109.2738 [hep-ph]].
- [52] H. Hatanaka and K. C. Yang, *Eur. Phys. J. C* **67** (2010) 149–162, arxiv: [0907.1496 [hep-ph]].
- [53] Cai. Dian. Lu and Wei. Wang, “Analysis of $B \rightarrow K_7^*(\rightarrow K\pi)\mu^+\mu^-$ in the higher kaon resonance region”, *Phys. Rev. D* **85**, no.3, 034014, (2012) [arXiv:1111.1513 [hep-ph]].

- [54] D. Das, B. Kindra, G. Kumar and N. Mahajan, Phys. Rev. D **99** (2019) no.9, 093012 [arXiv:1812.11803 [hep-ph]].
- [55] A. Donnachie, E. R. Berger, H. G. Dosch and O. Nachtmann, Eur. Phys. J. C **14**, no.4, 673-682 (2000), [arXiv:0001270 [hep-ph]].
- [56] A. J. Buras, M. Munz, Phys. Rev. D **52**, 186–195 (1995) [arXiv:9501281 [hep-ph]].
- [57] A. Ali, P. Ball, L. T. Handoko and G. Hiller, Phys. Rev. D **61**, 074024(2000).
- [58] A. Faessler, T. Gutsche, M. A. Ivanov, J. G. Korner and V. E. Varley, Eur. Phys. J. direct **4**, no. 1, 18 (2002), [arXiv:0205287[hep-ph]].
- [59] Y. G. Kim, T. Morozumi, C. S. Kim, and C. D. Lü Phys. Rev. D **62**, no.3, 034013 (2000) [arXiv:0001151 [hep-ph]].
- [60] Z. G. Wang Mod. Phys. Lett. A **26**, 2761-2782 (2011) [arXiv:1011.3200 [hep-ph]].
- [61] H. Y. Cheng, Y. Koike and K. C. Yang Phys. Rev. D **82**, 054019 (2010) [arXiv:1007.3541 [hep-ph]].
- [62] T. M. Aliev, H. Dag, A. Kokulu and A. Ozpineci, Phys. Rev. D **100**, no.9, 094005 (2019) [arXiv:1908.00847[hep-ph]].
- [63] M. J. Dugan and B. Grinstein “QCD basis for factorization in decays of heavy mesons”, Phys. Lett. **B255**, 583-588, 1991.
- [64] M. Wirbel, B. Stech, and M. Bauer, Z. Phys. C **29**, 637 (1985).
- [65] Y. B. Zuo, C. X. Yue, B. Yu, Y. H. Kou, Y. Chen and W. Ling, Eur. Phys. J. C **81**, no.1, 30 (2021)
- [66] N. Rajeev, N. Sahoo and R. Dutta, Phys. Rev. D **103**, 095007 (2021), [arXiv:2009.06213 [hep-ph]].
- [67] S. Descotes-Genon, J. Matias, M. Ramon and J. Virto, JHEP **01**, 048 (2013), [arXiv:1207.2753 [hep-ph]].
- [68] S. Descotes-Genon, T. Hurth, J. Matias and J. Virto, JHEP **05**, 137 (2013), [arXiv:1303.5794 [hep-ph]].
- [69] C. Bobeth, T. Ewerth, F. Kruger and J. Urban, Phys. Rev. D **64**, 074014 (2001) [arXiv:0104284 [hep-ph]].
- [70] A. Arbey, T. Hurth, F. Mahmoudi, S. Neshatpour, Phys. Rev. D **98**, no.9, 095027 (2018) [arXiv:1806.02791[hep-ph]].
- [71] M. Aaboud *et al.* [ATLAS], JHEP **04** (2019), 098 [arXiv:1812.03017 [hep-ex]].
- [72] A. M. Sirunyan *et al.* [CMS], JHEP **04** (2020), 188 [arXiv:1910.12127 [hep-ex]].
- [73] R. Aaij *et al.* [LHCb], Phys. Rev. Lett. **118** (2017) no.19, 191801 [arXiv:1703.05747 [hep-ex]].
- [74] [ATLAS], ATLAS-CONF-2020-049.
- [75] R. Aaij *et al.* [LHCb], [arXiv:2108.09283 [hep-ex]].
- [76] T. Hurth and F. Mahmoudi, JHEP **04**, 097 (2014), [arXiv:1312.5267 [hep-ph]].
- [77] [CMS], CMS-PAS-BPH-21-006.
- [78] A. Crivellin, L. Hofer, J. Matias, U. Nierste, S. Pokorski and J. Rosiek, Phys. Rev. D **92** no.5, 054013 (2015) doi:10.1103/PhysRevD.92.054013 [arXiv:1504.07928 [hep-ph]].
- [79] A. K. Alok, A. Dighe, S. Gangal and D. Kumar, Eur. Phys. J. C **80**, no.7, 682 (2020) [arXiv:1912.02052 [hep-ph]].
- [80] A. K. Alok, N. R. S. Chundawat and D. Kumar, Eur. Phys. J. C **82**, no.1, 30 (2022) [arXiv:2110.12451 [hep-ph]].
- [81] L. Di Luzio, M. Kirk, A. Lenz and T. Rauh, JHEP **12**, 009(2019), [arXiv:1909.11087 [hep-ph]].
- [82] W. Altmannshofer, S. Gori, J. Martín-Albo, A. Sousa and M. Wallbank, Phys. Rev. D **100** (2019) no.11, 115029, [arXiv:1902.06765 [hep-ph]].
- [83] S. R. Mishra *et al.* [CCFR], Phys. Rev. Lett. **66** (1991), 3117-3120
- [84] F. James and M. Roos, Comput. Phys. Commun. **10**, 343-367 (1975).
- [85] W. Detmold, S. Meinel, Phys. Rev. D, textbf93, no.7, 074501(2016).
- [86] M. Tanabashi *et al.*, Phys. Rev. D **98**, no.3, 030001 (2018).